Procedia Computer Science

Volume 80, 2016, Pages 1267–1278

ICCS 2016. The International Conference on Computational Science

Uncertainty Quantification of Parameters in SBVPs Using Stochastic Basis and Multi-Scale Domain Decomposition

Victor Ginting[1], Bradley McCaskill[1], and Prosper Torsu[1]

University of Wyoming
Laramie, WY 82071
vginting@uwyo.edu
bmccaski@uwyo.edu
ptorsu@uwyo.edu

Abstract

Quantifying uncertainty effects of coefficients that exhibit heterogeneity at multiple scales is among many outstanding challenges in subsurface flow models. Typically, the coefficients are modeled as functions of random variables governed by certain statistics. To quantify their uncertainty in the form of statistics (e.g., average fluid pressure or concentration) MC methods have been used. In a separate direction, multi-scale numerical methods have been developed to efficiently capture spatial heterogeneity that otherwise would be intractable with standard numerical techniques. Since heterogeneity of individual realizations can drastically differ, a direct use of multi-scale methods in MC simulations is problematic. Furthermore, MC methods are known to be very expensive as a lot of samples are required to adequately characterize the random component of the solution. In this study, we utilize a stochastic representation method that exploits the solution structure of the random process in order to construct a problem dependent stochastic basis. Using this stochastic basis representation a set of coupled yet deterministic equations is constructed. To reduce the computational cost of solving the coupled system, we develop a multi-scale domain decomposition method utilizing Robin transmission conditions. In the proposed method, enrichment of the solution space can be performed at multiple levels that offer a balance between computational cost, and accuracy of the approximate solution.

Keywords: Stochastic PDE, MC Simulation, Multi-scale Domain Decomposition

1 Introduction

Many physical and engineering phenomena involve parameters which cannot be precisely measured. This introduces uncertainty that propagates to quantities of interest that depend on the parameters. To incorporate the uncertainty into realistic models, the parameters are modeled as functions of random variables that follow certain statistical descriptions. To this end, the original governing differential equations modeling the phenomena are reformulated as stochastic differential equations (SDEs). Standard practice is to use Monte-Carlo (MC) simulations

Selection and peer-review under responsibility of the Scientific Programme Committee of ICCS 2016

doi:10.1016/j.procs.2016.05.500

[9, 7] whereby a set of samples of the parameters are created and the resulting statistics of the quantities of interest can be gathered. For realistic statistical information, a lot of realizations of the quantities of interest are needed. Although MC methods are direct, stable and easy to use, they can be extremely expensive. This is attributed to the slow convergence rate, namely, $\mathcal{O}(1/\sqrt{N_{\rm mc}})$, where $N_{\rm mc}$ is the number of samples committed to the simulation.

This drawback has given rise to some intrusive and nonintrusive methods. Nonintrusive methods aim at providing alternative solution techniques whilst intrusive methods are designed to accelerate the convergence rate of the MC method. For example, the Multilevel MC [4] is a variance reduction technique geared toward achieving a high convergence rate of the MC method. It utilizes the linearity property of the expectation operator to capture most of the variability on coarse grids. This significantly reduces the cost associated with the traditional MC method as fewer samples are needed to achieve the same accuracy. Additionally, generalized polynomial chaos [11], inspired by Wiener in the late thirties, is another novel solution method. The idea is to characterize a random quantity with respect to another random variable with a known distribution. In its earliest development the polynomial chaos is a spectral decomposition of Gaussian random variables in terms of orthogonal Hermite polynomials. However, the Hermite expansion is limited to only random processes with finite second-order moments [2].

In lieu of recent efforts to develop robust and efficient methods, it remains a challenging task to provide approximate solutions to SDEs. The situation is exacerbated when it is a necessity to account for the parameters' uncertainty in an optimization problem. A typical optimization scheme utilizes some iterative procedure that is aimed at gathering certain variables by finding extremal values of certain objective functions. Within this framework, the objective functions are written in terms some statistics of the quantities of interest which depend on the uncertain parameters. The obvious scenario is to place a MC simulation within the iterative procedure. It is not difficult to realize that the overall procedure can be intractable, especially when $N_{\rm mc}$ is large enough to account for the uncertainty and many iterations are needed to drive the optimization process to an acceptable convergence criterion.

This work is motivated by the aforementioned predicament. In particular, we propose and test a systematic method to avoid MC simulations in optimization problems that require proper incorporation of parameters' uncertainty. While specific discussions of optimization procedures is outside the scope of this paper, once the proposed method is available, its inclusion in the optimization problems is straightforward. To fix the idea in the proper setting, we consider the problem of well optimization in a subsurface flow simulation (e.g. [1]), in which given uncertainty in the permeability and existing well configuration, the end result is to derive the optimal new location constrained by appropriate objective functions. The governing model is

$$\begin{aligned} -\nabla\cdot\big(k(\boldsymbol{x},\omega)\,\nabla u(\boldsymbol{x},\omega)\big) &= f(\boldsymbol{x}) \quad \boldsymbol{x}\in\mathcal{D},\ \omega\in\Omega \\ -k(\boldsymbol{x},\omega)\,\nabla u(\boldsymbol{x},\omega)\cdot\boldsymbol{n} &= g(\boldsymbol{x}) \quad \text{on } \partial\mathcal{D}, \end{aligned} \tag{1}$$

where u is the subsurface pressure (the quantity of interest), $\mathcal{D}\subset\mathbb{R}^2$ is a bounded domain and ω is a random parameter and we assume that compatibility condition is satisfied; namely

$$\int_{\mathcal{D}} f(\boldsymbol{x})\,\mathrm{d}\boldsymbol{x} = \int_{\partial\mathcal{D}} g(\boldsymbol{x})\,\mathrm{d}\boldsymbol{l}. \tag{2}$$

The well location is represented by $\boldsymbol{x}$ in $f(\boldsymbol{x})$, so within the optimization process, this is the sought variable, which can be parametrized by certain conditions. As alluded to earlier, we will not deal with the optimization itself, instead the focus is on the construction of a robust method to replace the MC simulations in the optimization. We assume the availability of permeability

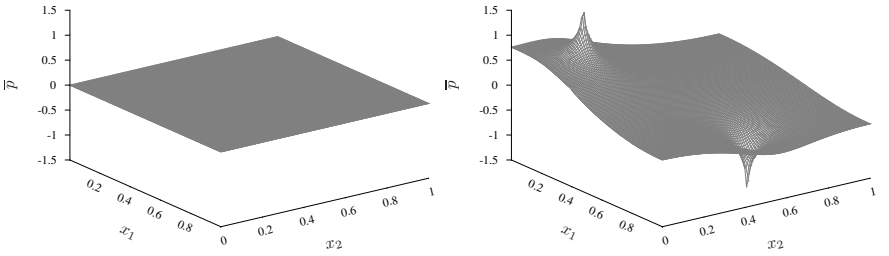

Figure 1: Average permeability solution vs Monte Carlo simulation (right)

samples $\{k(\boldsymbol{x},\omega_i)\}_{i=1}^{N_{\rm mc}}$ that is obtained from prior subsurface characterization that honors past measurement data.

As noted earlier, MC simulations can be extremely expensive because for every permeability sample, (1) must be solved numerically for the corresponding pressure sample. Furthermore, realistic geostatistical models from which permeability samples are obtained dictate spatial heterogeneity of the realizations, culminating in high dimensional algebraic systems which must be solved to get the pressure samples. An obvious but unreliable substitute for MC simulations is a one time calculation of the pressure in (1) with the sample average of the permeability, $\overline{k}(\boldsymbol{x})$, replacing $k(\boldsymbol{x},\omega)$. To illustrate potential discrepancy in the pressure statistics, in particular average pressure $\overline{p}$, we gather $N_{\rm mc} = 10000$ permeability fields and set $f(\boldsymbol{x})$ to be a combination of Dirac Delta functions representing two wells. We assume homogeneous boundary conditions, $g(\boldsymbol{x}) = 0$, and solve (1) with this approach and compare it with the usual MC simulation. Figure 1 illustrates this comparison. The left plot is the pressure profile resulting from solving (1) using $\overline{k}(\boldsymbol{x})$ as the data, while the right plot shows the average of pressure samples found with a Monte Carlo simulation. We note that the plot on the left is not identically zero. Clearly, this approach yields a result that completely deviates from the MC average.

The proposed method offers two major features: (1) the avoidance of MC simulations through construction of a deterministic system and (2) efficient incorporation of spatial heterogeneity in the resulting system. Item (1) is accomplished in the framework of a stochastic Galerkin approach which is described in Section 2. Item (2) is realized by employing a MsR method which is presented in Section 3. The application of a multi-scale method in this framework is particularly appealing to tackle the curse of dimensionality that is commonly a major drawback of the Stochastic Galerkin approach. Section 4 provides a set of numerical experiments to test the efficacy of the proposed method. A conclusion is presented in Section 5.

2 A Stochastic Galerkin Formulation

The stochastic Galerkin approach is based on a variational formulation associated with (1). To proceed, we consider the usual probability space $(\Omega,\mathcal{F},P)$ where Ω denote the sample space, $\mathcal{F}$ the σ-algebra of Ω and P, a probability measure on $\mathcal{F}$. We shall work with second order random fields, namely, all functions $v : \mathcal{D}\times\Omega \to \mathbb{R}$ such that

$$\int_\Omega \int_{\mathcal{D}} v^2(\boldsymbol{x},\omega)\,\mathrm{d}\boldsymbol{x}\mathrm{d}P(\omega) = E\big[||v||^2_{L^2(\mathcal{D})}\big] < \infty.$$

In a variational framework, we assume that there exist constants $k_{\min}, k_{\max} \in (0,\infty)$ such that

$$k_{\min} \le k(\boldsymbol{x},\omega) \le k_{\max} \quad \text{a.e in} \quad \mathcal{D}\times\Omega. \tag{1}$$

Now, define

$$V = \Big\{ v : \mathcal{D} \times \Omega \to \mathbb{R} : \quad \|v\|_V < \infty, \ \int_{\mathcal{D}} v(\boldsymbol{x}, \omega)\, \mathrm{d}\boldsymbol{x} = 0 \Big\} \ , \ \ \|v\|_V = \sqrt{E\Big[||\nabla v||^2_{L^2(\mathcal{D})} \Big]}. \quad (2)$$

Also, define the bilinear form $a : V \times V \to \mathbb{R}$ and the linear functional $\ell : V \to \mathbb{R}$ by

$$\begin{aligned} a(w, v) &= E\Big[\int_{\mathcal{D}} k(\boldsymbol{x}, \cdot) \nabla w(\boldsymbol{x}, \cdot) \cdot \nabla v(\boldsymbol{x}, \cdot)\, \mathrm{d}\boldsymbol{x} \Big] \ \text{ and} \\ \ell(v) &= E\Big[\int_{\mathcal{D}} f(\boldsymbol{x})\, v(\boldsymbol{x}, \cdot)\, \mathrm{d}\boldsymbol{x} - \int_{\partial\mathcal{D}} g(\boldsymbol{x}) v(\boldsymbol{x}, \cdot)\, \mathrm{d}\boldsymbol{l} \Big]. \end{aligned} \quad (3)$$

Then, one can easily verify that V is a Hilbert space equipped with the inner product $a(\cdot, \cdot)$. Assuming coercivity and boundedness of $a(\cdot, \cdot)$ and boundedness of ℓ in V, Lax-Milgram's theorem guarantees the existence of a unique u in V satisfying

$$a(u, v) = \ell(v) \ \ \text{for all} \ \ v \ \text{in} \ V. \quad (4)$$

The stochastic Galerkin approach relies on the variational formulation (4). Specifically, it depends on the construction of a subspace of V inside which (4) is imposed. To do this, given a positive integer N_{sb} we first set

$$\mathcal{W} = \Big\{ \boldsymbol{v} = (v_0, v_1, \cdots, v_{N_{\text{sb}}}) : v_i \in H^1(\mathcal{D}), \int_{\mathcal{D}} \boldsymbol{v}(\boldsymbol{x})\, \mathrm{d}\boldsymbol{x} = \boldsymbol{0} \ \Big\}. \quad (5)$$

Given a stochastic basis $\Big\{ \mathcal{B}_i(\omega) \Big\}_{i=0}^{N_{\text{sb}}}$, we define $\mathcal{V}$ as

$$\mathcal{V} = \Big\{ v : \mathcal{D} \times \Omega \to \mathbb{R};\ v = \boldsymbol{\mathcal{B}}(\omega) \cdot \boldsymbol{v},\ \boldsymbol{v} \in \mathcal{W} \Big\}, \ \text{ with } \ \boldsymbol{\mathcal{B}}(\omega) = \Big(\mathcal{B}_0(\omega), \mathcal{B}_1(\omega), \cdots, \mathcal{B}_{N_{\text{sb}}}(\omega) \Big), \quad (6)$$

where $\boldsymbol{v} \cdot \boldsymbol{w}$ is the usual Euclidian inner product in $\mathbb{R}^{N_{\text{sb}}+1}$. We note that if v is in $\mathcal{V}$, then

$$\|v\|_V^2 = \sum_{i=0}^{N_{\text{sb}}} \sum_{j=0}^{N_{\text{sb}}} E[\mathcal{B}_i \mathcal{B}_j] \int_{\mathcal{D}} \nabla v_i \cdot \nabla v_j\, \mathrm{d}\boldsymbol{x} \ \leq \ \sum_{i=0}^{N_{\text{sb}}} \sum_{j=0}^{N_{\text{sb}}} E[\mathcal{B}_i \mathcal{B}_j] \ |v_i|_1 \ |v_j|_1,$$

where $|\cdot|_1$ is the usual semi-norm on $H^1(\mathcal{D})$. Therefore, as long as $E[\mathcal{B}_i \mathcal{B}_j]$ is finite, $\mathcal{V}$ is a subspace of V. In particular, if $\Big\{ \mathcal{B}_j \Big\}_{j=0}^{N_{\text{sb}}}$ are uncorrelated and $E[\mathcal{B}_i \mathcal{B}_j] = \delta_{ij}$, then $\|v\|_V^2 = \sum_{j=0}^{N_{\text{sb}}} |v_i|_1^2$. In light of the above variational setting, we seek $u_{N_{\text{sb}}}$ in $\mathcal{V}$ such that

$$a(u_{N_{\text{sb}}}, v) = \ell(v) \ \ \text{for all} \ \ v \ \text{in} \ \mathcal{V}. \quad (7)$$

Two important facts that accompany this stochastic continuous Galerkin formulation are (1). Galerkin Orthogonality which follows trivially; and (2). Céa's lemma that allows for establishing the convergence of $u_{N_{\text{sb}}}$ to u based on the quality of the approximation subspace, $\mathcal{V}$.

Now, by setting $u_{N_{\text{sb}}} = \boldsymbol{\mathcal{B}} \cdot \boldsymbol{u}$ for $\boldsymbol{u}$ in $\mathcal{W}$ and replacing v by $\mathcal{B}_j v_j$ in $\mathcal{V}$ for every $j = 0, 1, \cdots N_{\text{sb}}$, we see that (7) is transformed into finding $\boldsymbol{u}$ in $\mathcal{W}$ satisfying

$$A(\boldsymbol{u}, \boldsymbol{v}) = F(\boldsymbol{v}) \quad \text{for all} \ \ \boldsymbol{v} \ \text{in} \ \mathcal{W}, \quad (8)$$

$$\text{where} \quad A(\boldsymbol{w},\boldsymbol{v}) = \sum_{j=0}^{N_{\rm sb}}\sum_{i=0}^{N_{\rm sb}} \int_{\mathcal{D}} E\Big[k\mathcal{B}_i\mathcal{B}_j\Big]\nabla w_j\cdot\nabla v_i\,\mathrm{d}\boldsymbol{x}$$

$$\text{and} \quad F(\boldsymbol{v}) = \sum_{i=0}^{N_{\rm sb}} E\Big[\mathcal{B}_i\Big]\Big(\int_{\mathcal{D}} f\,v_i\,\mathrm{d}\boldsymbol{x} - \int_{\partial\mathcal{D}} g v_i\,\mathrm{d}\boldsymbol{l}\Big).$$

Once the solution of (8) has been found, approximate value for $E[u(\boldsymbol{x})]$ can be calculated. In particular, by further assumming that $E[\mathcal{B}_i] = \delta_{0i}$, we have $E[u(\boldsymbol{x})] \approx E[u_{N_{\rm sb}}] = E[\boldsymbol{\mathcal{B}}\cdot\boldsymbol{u}] = u_0$, where u_0 is the first entry in $\boldsymbol{u}$ of (8).

The approximation that we have developed in this section can be thought of as a semi-discretization of (4), i.e., discretization with respect to the probability/uncertainty space. However, it is circumstantially rare to find the actual solution of (8), and thus (7). Consequently, one has to devise a full-discretization for the approximate solution of (4). This is achieved by employing a spatial discretizations on (8), which is discussed in the next section.

3 Numerical Approximations of $u_{N_{\rm sb}}$

3.1 Continuous Galerkin Finite Element Method

We begin by assuming that the domain $\mathcal{D}$ is contained in $\mathbb{R}^2$ and is polygonal in shape. We then construct a triangulation of $\mathcal{D}$, denoted by $\mathcal{T}_h$, consisting of polygonal elements τ such that $\mathcal{D} = \cup_{\tau\in\mathcal{T}_h}\tau$. Furthermore, for each $\tau\in\mathcal{T}_h$ we require that $0 < \mathrm{diam}(\tau) \le h$, and $\tau_i\cap\tau_j = \varnothing$ for every distinct $\tau_i,\tau_j\in\mathcal{T}_h$. Next we define a space $\mathcal{W}_h\subset\mathcal{W}$ consisting of all continuous functions that are linear on each polygonal $\tau\in\mathcal{T}_h$. More specifically, we define

$$\mathcal{W}_h = \Big\{\boldsymbol{v}_h\in C(\overline{\mathcal{D}})^{N_{\rm sb}+1} : \boldsymbol{v}_h\in(\mathcal{P}_1(\tau))^{N_{\rm sb}+1},\ \forall\tau\in\mathcal{T}_h \text{ and } \int_{\mathcal{D}}\boldsymbol{v}_h(\boldsymbol{x})\,\mathrm{d}\boldsymbol{x} = \boldsymbol{0}\Big\}, \tag{9}$$

where $\mathcal{P}_1(\tau)$ is the space of linear functions in τ. The finite element approximation of the solution to (8) is to find $\boldsymbol{u}_h\in\mathcal{W}_h$ satisfying

$$A(\boldsymbol{u}_h,\boldsymbol{v}_h) = F(\boldsymbol{v}_h) \quad \text{for all} \quad \boldsymbol{v}_h \text{ in } \mathcal{W}_h. \tag{10}$$

3.2 Construction of the Multi-scale Robin (MsR) Solution Space

In practice a direct application of traditional finite elements to many physical and engineering may be unsuitable. Particularly, porous media flow models can present a distinct challenge since many rock properties tend to be multi-scale in nature. For instance, if the magnitude of a permeability profile changes by many orders of magnitude over small distances, the finite element approximation may require a very fine triangulation $\mathcal{T}_h$. In such cases the resulting system can be both ill-conditioned and computationally expensive to invert. To alleviate this burden, we propose to use the MsR method to solve (8). The development of the MsR method is deeply rooted in existing and well documented iterative substructuring domain decomposition methods [6, 8]. In contrast, we avoid the traditional iteration by expressing the solution in terms of multi-scale basis functions whose local variational formulation is discussed in this section.

Given $\mathcal{T}_h$ described in section 3.1 we decompose the global domain $\mathcal{D}$ into a set of non-overlapping subdomains $\mathcal{N}_H = \{\mathcal{D}_m\}_{m=1}^{N_{\rm sd}}$, where $h < H$, and each $\mathcal{D}_m$ is the union of a subset of $\mathcal{T}_h$. Consequently, each $\mathcal{D}_m$ maintains conformity with the underlying fine scale discretization. It is on this set of subdomains which we will construct a set of local variational formulations governing the multi-scale basis functions. Let $\mathcal{N}_{m,H}\subset\mathcal{N}_H$ represent the set of subomains

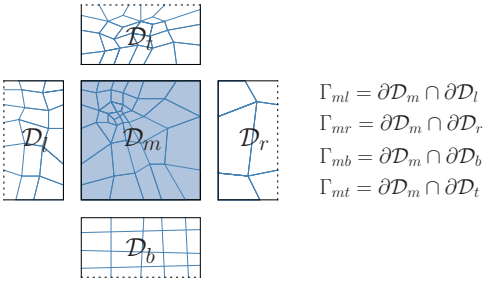

Figure 2: A rectangular subdomain $\mathcal{D}_m$ and its neighbouring subdomains $\mathcal{N}_{m,H}$

sharing a boundary with subdomain $\mathcal{D}_m$. For example, the set $\mathcal{N}_{m,H} = \{\mathcal{D}_l, \mathcal{D}_r, \mathcal{D}_b, \mathcal{D}_t\}$ is associated with the subdomain presented in Figure 3.2.

For each $\mathcal{D}_n \in \mathcal{N}_{m,H}$ we decompose the boundary $\Gamma_{mn} = \partial\mathcal{D}_m \cap \partial\mathcal{D}_n$ into a set of segments $\{I^i_{mn}\}_{i=1}^{k_{mn}}$, such that $I^i_{mn} \cap I^j_{mn} = \varnothing$ if $i \neq j$. Furthermore, we denote $\{z^i_{mn}\}_{i=0}^{k_{mn}}$ to be the set of points on the boundary which lie between these segments. It is worth noting that the accuracy of the resulting MsR approximation will be dependent on the length of these segments $\{I^i_{mn}\}_{i=1}^{k_{mn}}$. For later discussion we define $\widetilde{h} \in [h, H]$ to be such that $0 < |I^i_{mn}| \leq \widetilde{h}$. In addition, for ease of notation we define

$$\mathcal{S}_m = \left\{ z^i_{mn} : i \in \{0, 1, \cdots k_{mn}\}, \mathcal{D}_n \in \mathcal{N}_{m,H} \right\}.$$

Designate the triangulation of $\mathcal{D}_m$ by $\mathcal{T}_{m,h}$, the set consisting of the polygonal elements $\tau \in \mathcal{T}_h$ such that $\mathcal{D}_m = \cup_{\tau \in \mathcal{T}_{m,h}} \tau$. Next we define a space $\mathcal{W}^m_h \subset H^1(\mathcal{D}_m)^{N_{\rm sb}+1}$ consisting of all continuous functions that are linear on each polygonal $\tau \in \mathcal{T}_{m,h}$. That is to say,

$$\mathcal{W}^m_h = \left\{ \boldsymbol{v}_h \in C(\overline{\mathcal{D}_m})^{N_{\rm sb}+1} : \boldsymbol{v}_h \in (\mathcal{P}_1(\tau))^{N_{\rm sb}+1}, \ \forall \tau \in \mathcal{T}_{m,h} \right\}. \tag{11}$$

Next, set $\{\varphi^\eta\}_{\eta \in \mathcal{S}_m} \subset \mathcal{W}^m_{\widetilde{h}} \subseteq \mathcal{W}^m_h$ such that they are the usual tent functions associated with $\mathcal{S}_m$ on their respective compact supports.

To characterize the MsR approximation we associate to each subdomain a set of multi-scale basis functions $\{\boldsymbol{\psi}^\eta_k : k \in \{0, \ldots, N_{\rm sb}\}, \eta \in \mathcal{S}_m\}$ where each $\boldsymbol{\psi}^\eta_k \in \mathcal{W}^m_h$ satisfies

$$A_m(\boldsymbol{\psi}^\eta_k, \boldsymbol{v}) + \sum_{\mathcal{D}_n \in \mathcal{N}_{m,H}} b_{mn}(\boldsymbol{\psi}^\eta_k, \boldsymbol{v}) = r^\eta_k(\boldsymbol{v}) \quad \forall \boldsymbol{v} \in \mathcal{W}^m_h, \tag{12}$$

with

$$\begin{aligned} A_m(\boldsymbol{w}, \boldsymbol{v}) &= \sum_{j=0}^{N_{\rm sb}} \sum_{i=0}^{N_{\rm sb}} \int_{\mathcal{D}_m} E\Big[k\mathcal{B}_i\mathcal{B}_j\Big] \nabla w_j \cdot \nabla v_i \, \mathrm{d}\boldsymbol{x}, \\ b_{mn}(\boldsymbol{w}, \boldsymbol{v}) &= -\int_{\Gamma_{mn}} \gamma_{mn} \boldsymbol{w} \cdot \boldsymbol{v} \, \mathrm{d}\boldsymbol{l}, \ \text{ and } \ r^\eta_k(\boldsymbol{v}) = \int_{\partial\mathcal{D}_m} \varphi^\eta \boldsymbol{e}_k \cdot \boldsymbol{v} \, \mathrm{d}\boldsymbol{l}, \end{aligned} \tag{13}$$

where $\boldsymbol{e}_k$ is the k-th standard unit vector and γ_{mn} is some positive constant. In addition, we define $\hat{\boldsymbol{\psi}}^m \in \mathcal{W}^m_h$ to be the shape function which satisfies

$$A_m(\hat{\boldsymbol{\psi}}^m, \boldsymbol{v}) + \sum_{\mathcal{D}_n \in \mathcal{N}_{m,H}} b_{mn}(\hat{\boldsymbol{\psi}}^m, \boldsymbol{v}) = F_m(\boldsymbol{v}) \quad \forall \boldsymbol{v} \in \mathcal{W}^m_h, \tag{14}$$

where

$$F(\boldsymbol{v}) = \sum_{i=0}^{N_{\rm sb}} E\Big[\mathcal{B}_i\Big]\Big(\int_{\mathcal{D}_m} f\, v_i \,\mathrm{d}\boldsymbol{x} - \int_{\partial\mathcal{D}\cap\partial\mathcal{D}_m} g v_i \,\mathrm{d}\boldsymbol{l}\Big). \tag{15}$$

Observe that linear independence of $\widetilde{\mathcal{W}}_h^m = \{\hat{\boldsymbol{\psi}}^m, \boldsymbol{\psi}_k^\eta : k \in \{0,\ldots,N_{\rm sb}\}, \eta \in \mathcal{S}_m\}$ is inherited from the structure of $\{\varphi^\eta\}_{\eta\in\mathcal{S}_m}$. Furthermore, since the multi-scale basis functions are found in $\mathcal{W}_h^m$ we see that $\widetilde{\mathcal{W}}_h^m \subset \mathcal{W}_h^m$. Consequently, the size of $\widetilde{h}$, the resolution of the multi-scale basis functions, has a direct effect on the accuracy of the resulting approximate solution. We will explore this relationship further in the numerical examples section.

On the global domain $\mathcal{D}$, we now define the MsR solution space to be

$$\widetilde{\mathcal{W}}_h = \{\boldsymbol{v} = (v_0, v_1, \cdots, v_{N_{\rm sb}}) : v_i \in H^1(\mathcal{D}), \boldsymbol{v}|_{\mathcal{D}_m} \in \widetilde{\mathcal{W}}_h^m\}. \tag{16}$$

It is in this space of functions which we will seek the MsR approximation of the global solution $\boldsymbol{u}$ which satisfies (8). To this end we choose to express the MsR approximation as

$$\widetilde{\boldsymbol{u}} = \sum_{m=1}^{N_{\rm sd}} \widetilde{\boldsymbol{u}}_m\, \chi_{\mathcal{D}_m} \quad \text{with} \quad \widetilde{\boldsymbol{u}}_m = \sum_{k=0}^{N_{\rm sb}} \sum_{\eta\in S} \alpha_k^\eta \boldsymbol{\psi}_k^\eta + \hat{\boldsymbol{\psi}}^m. \tag{17}$$

3.3 The MsR Method

In the MsR method, local representations $\widetilde{\boldsymbol{u}}_m$ are found in each space $\widetilde{\mathcal{W}}_h^m$ which approximate the solution of (8). In order to construct an algebraic system governing the multi-scale approximation we impose a sense of continuity of each local approximation across the subdomain boundaries. Specifically, on each boundary Γ_{mn} we choose to establish continuity of both the local solutions and their fluxes. This is accomplished by imposing the following Robin transmission condition:

$$\begin{aligned}\sum_{i,j=0}^{N_{\rm sb}} \int_{\Gamma_{mn}} \Big(- E[k\mathcal{B}_i\mathcal{B}_j]\nabla\widetilde{u}_{m,j}\cdot\boldsymbol{n} - \gamma_{mn}\widetilde{u}_{m,j}\Big) v_i \,\mathrm{d}\boldsymbol{l} \\ = \sum_{i,j=0}^{N_{\rm sb}} \int_{\Gamma_{mn}} \Big(E[k\mathcal{B}_i\mathcal{B}_j]\nabla\widetilde{u}_{n,j}\cdot\boldsymbol{n} - \gamma_{mn}\widetilde{u}_{n,j}\Big) v_i \,\mathrm{d}\boldsymbol{l}.\end{aligned} \tag{18}$$

By requiring (18) to be satisfied on each interface boundary an appropriate representation of the multiscale Robin approximation can be devised. Consequently, we observe that $\widetilde{\boldsymbol{u}}_m$ will satisfy

$$A_m(\widetilde{\boldsymbol{u}}_m, \boldsymbol{v}) + \sum_{\mathcal{D}_n\in\mathcal{N}_{m,H}} b_{mn}(\widetilde{\boldsymbol{u}}_m, \boldsymbol{v}) = \sum_{\mathcal{D}_n\in\mathcal{N}_{m,H}} \widetilde{r}_{mn}(\boldsymbol{v}) + F_m(\boldsymbol{v}) \quad \forall \boldsymbol{v} \in \mathcal{W}_h^m, \tag{19}$$

where

$$\widetilde{r}_{mn}(\boldsymbol{v}) = \int_{\Gamma_{mn}} \sum_{j=0}^{N_{\rm sb}} \sum_{i=0}^{N_{\rm sb}} \Big(E[k\mathcal{B}_i\mathcal{B}_j]\nabla\widetilde{u}_{n,j}\cdot\boldsymbol{n} - \gamma_{nm}\widetilde{u}_{n,j}\Big) v_i \,\mathrm{d}\boldsymbol{l}. \tag{20}$$

Using the linearity of the forms (13) and (15) we find that (19) is equivalent to

$$\sum_{k=0}^{N_{\rm sb}} \sum_{\eta\in\mathcal{S}_m} \alpha_k^\eta r_k^\eta(\boldsymbol{v}) \,\mathrm{d}\boldsymbol{l} = \sum_{\mathcal{D}_n\in\mathcal{N}_m} \widetilde{r}_{mn}(\boldsymbol{v}) \tag{21}$$

Furthermore, with some algebraic manipulation $\widetilde{r}_{mn}(\boldsymbol{v})$ can be rewritten as

$$\begin{aligned}\widetilde{r}_{mn}(\boldsymbol{v}) = -\sum_{k=0}^{N_{\text{sb}}}\sum_{\zeta\in\mathcal{S}_n}\alpha_k^{\zeta}\int_{\Gamma_{mn}} n\varphi^{\zeta}\boldsymbol{e}_k\cdot\boldsymbol{v}\,\mathrm{d}\boldsymbol{l} \\ -2\sum_{k=0}^{N_{\text{sb}}}\sum_{\zeta\in\mathcal{S}_n}\alpha_k^{\zeta}\int_{\Gamma_{mn}}\gamma_{mn}\boldsymbol{\psi}_k^{\zeta}\cdot\boldsymbol{v}\,\mathrm{d}\boldsymbol{l} - 2\int_{\Gamma_{mn}}\gamma_{mn}\hat{\boldsymbol{\psi}}^{n}\cdot\boldsymbol{v}\,\mathrm{d}\boldsymbol{l}.\end{aligned} \tag{22}$$

As a result, we now have a condition on the coefficients defining $\widetilde{\boldsymbol{u}}_m$ as well as $\widetilde{\boldsymbol{u}}_n$ for each $\mathcal{D}_n \in \mathcal{N}_{m,H}$. That is to say, we seek sets $\{\alpha_k^{\eta} : k \in \{0,\cdots N_{\text{sb}}\}, \eta \in \mathcal{S}_m\}$ and $\{\alpha_k^{\zeta} : k \in \{0,\cdots N_{\text{sb}}\}, \zeta \in \mathcal{S}_n\}$ for all $\mathcal{D}_n \in \mathcal{N}_{m,H}$ such that

$$\begin{aligned}\sum_{k=0}^{N_{\text{sb}}}\sum_{\eta\in\mathcal{S}_m}\alpha_k^{\eta}\int_{\partial\mathcal{D}_m}\varphi^{\zeta}\boldsymbol{e}_k\cdot\boldsymbol{v}\,\mathrm{d}\boldsymbol{l} + \sum_{k=0}^{N_{\text{sb}}}\sum_{\zeta\in\mathcal{S}_n}\alpha_k^{\zeta}\int_{\Gamma_{mn}}\varphi^{\zeta}\boldsymbol{e}_k\cdot\boldsymbol{v}\,\mathrm{d}\boldsymbol{l} \\ + 2\sum_{k=0}^{N_{\text{sb}}}\sum_{\zeta\in\mathcal{S}_n}\alpha_k^{\zeta}\int_{\Gamma_{mn}}\boldsymbol{\psi}_k^{\zeta}\cdot\boldsymbol{v}\,\mathrm{d}\boldsymbol{l} = -2\int_{\Gamma_{mn}}\hat{\boldsymbol{\psi}}^{n}\cdot\boldsymbol{v}\mathrm{d}\boldsymbol{l}\end{aligned} \tag{23}$$

for all $\boldsymbol{v} \in \mathcal{W}_h^m$.

By construction, elements of $\{\varphi^{\eta}\boldsymbol{e}_k : k \in \{0,\ldots,N_{\text{sb}}\}, \eta \in \mathcal{S}_m\}$ are elements of $\mathcal{W}_h^m$ so it is permissible to use them as test functions. Thus an algebraic system can be constructed governing the coefficients of the local MsR approximation. Indeed by constructing similar systems for each subdomain we observe that a algebraic system can be constructed which governs the value of all coefficients used to build the MsR approximation. Moreover, by our choice of test functions the resulting global system will be low dimensional.

4 Numerical Examples

To illustrate the proposed method we consider an application to well placement in an oil reservoir. We consider a test problem in which an injection well is placed at a fixed location. We then quantify the effect that choosing different locations for the production well has on the pressure

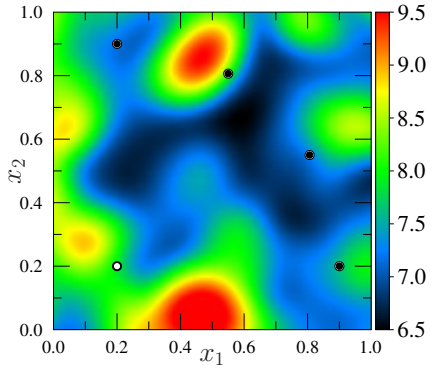

Figure 3: Logarithmic plot of the average permeability; the location of the injection well (white) and discharge wells (black).

	Time (min)		
$\widetilde{h}$	$H = 32h$	$H = 16h$	$H = 8h$
$2h$	13.1	3.3	1.2
$4h$	7.1	1.7	0.6
$8h$	4.3	1.1	0.4
$16h$	2.9	0.8	–
$32h$	2.2	–	–
	Reference: 1.3		

Table 1: Total time required to build multiscale basis functions and build global system for the MsR approximation using various subdomain dimensions (H) and segment lengths ($\widetilde{h}$). The time required to construct the linear algebra using CGFEM is used as reference.

profile by calculating its sample average. The locations of the injector and four production wells considered are presented in Figure 3.3. All calculations are performed on a 128×128 rectangular discretization of the domain $\mathcal{D} = [0,1] \times [0,1]$ (i.e, $h = 1/128$), with homogeneous Neumann boundary conditions. The permeability field is assumed to follow a log-normal distribution and to be isotropic with correlation length of 0.3 units. For these simulations 10000 samples of these permeability fields were generated. The average of the permeability samples is presented in Figure 3.3. Comparisons are made between the average of the pressure samples obtained using MC simulations, $\overline{u}_{\rm mc}$, and the stochastic basis representation using continuous Galerkin finite element, $\overline{u}_{\rm fe}$, and the MsR method, $\overline{u}_{\rm mr}$.

We now discuss construction of a stochastic basis $\{\mathcal{B}_i(\omega)\}_{i=0}^{N_{\rm sb}}$ that can be used in Section 2. The aim is to design a basis that reflects the uncertainty in the permeability. As mentioned in Section 1, this uncertainty has been relegated to the availability of $\{k(\boldsymbol{x},\omega_i)\}_{i=1}^{N_{\rm mc}}$, which in this case is generated with $N_{\rm mc} = 10000$. Thus, it suffices to produce a stochastic basis that reflect these permeability samples. However, a complication arises since the stochastic basis is to be generated from the inverse of the differential operator $-\nabla\cdot\big(k(\boldsymbol{x},\omega)\,\nabla\big)$. The approach adopted here is sampling-based, i.e., MC simulation. It begins with generation of response samples $\{w(\boldsymbol{x},\omega_i)\}_{i=1}^{N_{\rm mc}}$ to the permeability samples above by solving (1) $N_{\rm mc}$ times. Then, we calculate the samples covariance function

$$\mathcal{R}_w(\boldsymbol{x},\boldsymbol{y}) = \frac{1}{N_{\rm mc}}\sum_{i=1}^{N_{\rm mc}}\big(w(\boldsymbol{x},\omega_i)-\overline{w}(\boldsymbol{x})\big)\big(w(\boldsymbol{y},\omega_i)-\overline{w}(\boldsymbol{y})\big)\ , \quad \overline{w}(\cdot) = \frac{1}{N_{\rm mc}}\sum_{i=1}^{N_{\rm mc}} w(\cdot,\omega_i). \tag{24}$$

Clearly $\mathcal{R}_w(\boldsymbol{x},\boldsymbol{y}) = \mathcal{R}_w(\boldsymbol{y},\boldsymbol{x})$ and it belongs to $L^2(\mathcal{D}\times\mathcal{D})$. With this, we calculate the set of eigenpairs $\{\lambda_j,\phi_j\}_{j=1}^{N_{\rm sb}}$ that is governed by

$$\int_{\mathcal{D}} \mathcal{R}_w(\boldsymbol{x},\boldsymbol{y})\phi_j(\boldsymbol{y})\,{\rm d}\boldsymbol{y} = \lambda_j\phi_j(\boldsymbol{x}). \tag{25}$$

We note that the above integral operator is compact and self-adjoint, and thus the resulting

	Time (min)		
$\widetilde{h}$	$H = 32h$	$H = 16h$	$H = 8h$
$2h$	1.01	3.70	20.76
$4h$	0.19	0.66	5.80
$8h$	0.05	0.24	1.76
$16h$	0.02	0.07	–
$32h$	0.01	–	–
	MC: 21.5	Reference: 16.8	

Table 2: Average time to solve for the MsR approximation using various subdomain dimensions (H), and segment lengths ($\widetilde{h}$). As a references we present the average time to solve the linear algebra for the CGFEM, and the average time to run each MC simulation.

	DOF		
$\widetilde{h}$	$H = 32h$	$H = 16h$	$H = 8h$
$2h$	17136	42336	100800
$4h$	9072	23520	60480
$8h$	5040	14112	40320
$16h$	3024	9408	–
$32h$	2016	–	–
	Reference: 332820		

Table 3: Dimensions of the algebraic system for the MsR approximate with various subdomain dimensions (H), and segment lengths ($\widetilde{h}$). As a references we present the dimension of the algebraic system for the CGFEM approximation.

$\widetilde{h}$	$H = 32h$	$H = 16h$	$H = 8h$
$2h$	3.6	3.6	3.5
$4h$	3.6	3.6	4.0
$8h$	4.1	4.4	6.1
$16h$	11.1	10.7	–
$32h$	15.1	–	–
	Reference: 3.6	$\lvert\overline{u}_{\rm mc}\rvert_{H^1} = 2.1$	

Table 4: Relative difference of the average of the pressure samples found with the proposed method and MC simulation average using CGFEM average as reference.

eigenfunctions $\{\phi_j\}_{j=1}^{N_{\rm sb}}$ are orthonormal. Next, we set $\mathcal{B}_0(\omega_i) = 1$ for $i = 1, \cdots, N_{\rm mc}$, and

$$\mathcal{B}_j(\omega_i) = \int_{\mathcal{D}} \Big(w(\boldsymbol{x}, \omega_i) - \overline{w}(\boldsymbol{x}) \Big) \phi_j(\boldsymbol{x}) \, \mathrm{d}\boldsymbol{x}, \quad j = 1, \cdots, N_{\rm sb}, \ i = 1, \cdots, N_{\rm mc}. \tag{26}$$

It is obvious that $\overline{\mathcal{B}_j} = 0$ for $j \neq 0$ and by orthonormality of $\{\phi_j\}_{j=1}^{N_{\rm sb}}$, we have $\overline{\mathcal{B}_j \mathcal{B}_l} = \delta_{jl}$. Construction of stochastic basis in this manner has been done in [3, 12] for solving multi-query problems. In our numerical experiments, $\mathcal{R}_w(\boldsymbol{x}, \boldsymbol{y})$ is constructed with a forcing function $f(\boldsymbol{x}) = (x_1 - x_1^2)(x_2 - x_2^2) - 1/36$. The resulting stochastic basis has $N_{\rm sb} = 35$. The total computational time required to run this MC simulation, construct the stochastic basis and compute the coefficients $E[k\mathcal{B}_i\mathcal{B}_j]$ was approximately 58 minutes. In our experience this is the most computationally demanding component of the proposed method. It is worth noting that these calculations need only be performed once as a pre-processing step for the method. We also generated more stochastic basis functions than may be required to recover appropriate solutions for the simulation. This was done so that convergence rates of the method could be studied. In practice if $N_{\rm sb}$ is small, the computational cost of this pre-processing stage will be reduced. The values in the table correspond to the average over all four well configurations in Figure 3.3. The last stage of the pre-processing step required by the proposed method is the calculation of the multi-scale basis functions. It is worth noting that the calculation of these multi-scale basis functions is an embarrassingly parallel process. In particular, each set of local problems governing the multi-scale basis functions on a given subdomain is fully decoupled from those on other subdomains. In Table 1 we present a comparison of the total pre-processing time that was required for us to generate the multi-scale basis functions using various subdomain configurations H, and segment lengths $\widetilde{h}$.

The effect of the forcing function to the system is fully contained in the multi-scale basis functions $\{\hat{\boldsymbol{\psi}}^m\}_{m=1}^{N_{sd}}$. Thus, the construction of the global system governing the MsR approximation is a onetime computation. Indeed, when a new forcing function is considered one only

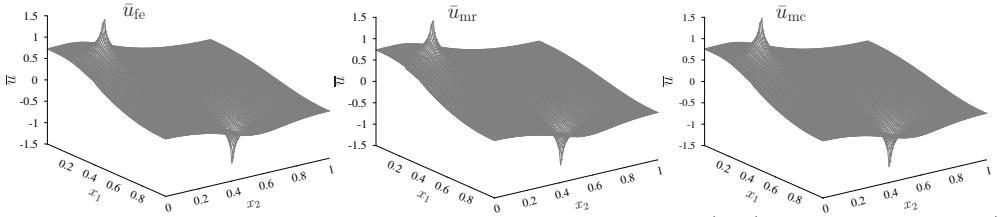

Figure 4: Average solution found with $N_{\rm sb} = 20$ using CGFEM (left), the MsR method ($H = \widetilde{h} = 16h$, middle), and MC simulation (right).

needs to compute a new set of shape functions $\{\hat{\psi}^m\}_{m=1}^{N_{sd}}$ and update the right hand side of (23) appropriately. In Table 2 we present the average time required to update these multi-scale basis functions and solve for the MsR approximation. Additionally, in Table 3 we present the number of degrees of freedom associated with the MsR approximation for various configurations of the method. Since the linear system governing the MsR approximation are typically low dimensional we choose to use a direct multi-frontal solver to invert the system (see for example [5]). However, in order to invert the higher dimensional linear system governing the CGFEM approximation we use a generalized minimum residual solver (see for example [10]).

During our numerical experiments we found that on average it takes approximately 22 minutes to complete one MC simulation with 10000 samples. If several well configurations need to be tested (such as in well optimization problems for which a set of MC simulations must be performed) then the overall computation time will be prohibitively long. In contrast for the initial cost involved with the pre-processing step of the proposed method, simulations of each well configuration can be performed in a fraction of the time.

A comparison of the average of the pressure samples found using all three methods discussed in this paper is presented in Figure 4. In all three cases we see considerable agreement of the profile structure. To demonstrate the performance of the MsR method we take the MC simulation average as a bench mark with which to test against. Specifically, we compute the magnitude of the difference between $\overline{u}_{\rm mc}$ and $\overline{u}_{\rm mr}$ in the H^1 semi-norm and divide the result by the magnitude of $\overline{u}_{\rm mc}$ in the H^1 semi-norm. In Table 4 we present the effect that various discretization choices can have on the resulting MsR approximation.

We observe that if $\widetilde{h}$ is resolved sufficiently close to the fine-scale the resulting difference with the reference average is small. In these cases the error of the resulting average is dominated by the stochastic basis representation of the probability space. However, as $\widetilde{h}$ is increased the error of the proposed method becomes dominated by what we call up-scaling error. Essentially, as fewer multi-scale basis functions are used to characterize the solution the effect of fine-scale features in the elliptic coefficients become poorly represented. However, at a practical level we have seen in Tables 1 and 2 that the computational cost of this method can be significantly reduced as $\widetilde{h}$ increases. Ultimately, there exists a balance between the accuracy and the efficiency of the proposed method.

In what follows, we numerically examine the interplay between the two main sources of error of the proposed method: the number of stochastic basis functions used to approximate the uncertainty space, and the degree of upscaling error introduced to the MsR approximation. In Figure 5 we summarize the results for one well configuration. We observed that irrespective of the amount of upscaling, the total error asymptotically decays as $N_{\rm sb}$ increases. Also confirmed by the figure is that the MsR approximation converges at a similar rate as the CGFEM method provided that the degree of up-scaling is sufficiently small. However, we do observe that as more upscaling error is introduced to the MsR approximation the convergence rate of the method deteriorates. Essentially, as the uncertainty space becomes better represented by the stochastic basis, upscaling error can become the dominate source of discrepancy. We also find that the method is stable and the H_1 relative differences decay monotonically.

5 Conclusion

An alternative method to the traditional MC simulations for quantifying uncertainty has been studied. The method explores possible ways of optimizing computational cost and available resources to produce accurate statistics of a stochastic quantity. In optimization problems, a one-time stochastic basis is calculated through excitation of the differential operator. For every stage of the optimization process, the stochastic basis and the multi-scale basis are reused. This significantly reduces computational cost and accelerates the rate of generating realizations to

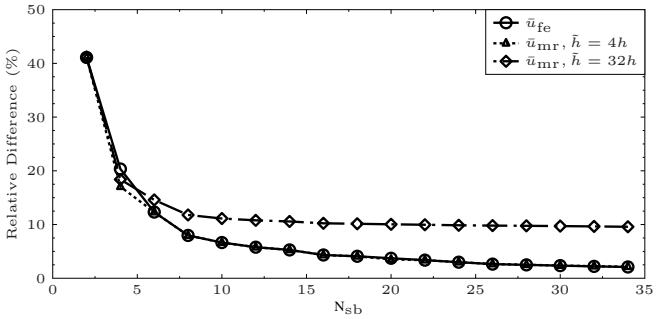

Figure 5: Relative H^1-difference of CGFEM and MsR approximations.

describe statistical properties of random processes. The method also provides the flexibility to further reduce computational cost by introducing some level of upscaling while maintaining accurate results. Our numerical examples have demonstrated that irrespective of other parameters, the MsR approximation gets more accurate as the number of stochastic basis increases. Moreover, accuracy of the solution could be mildly sacrificed for a substantial computational gain by adjusting the level of upscaling and number of subdomains.

References

[1] Vincent Artus, Louis J Durlofsky, Jérôme Onwunalu, and Khalid Aziz. Optimization of nonconventional wells under uncertainty using statistical proxies. *Computational Geosciences*, 10(4):389–404, 2006.

[2] Robert H Cameron and William T Martin. The orthogonal development of non-linear functionals in series of fourier-hermite functionals. *Annals of Mathematics*, pages 385–392, 1947.

[3] Mulin Cheng, Thomas Y Hou, Mike Yan, and Zhiwen Zhang. A data-driven stochastic method for elliptic pdes with random coefficients. *SIAM/ASA Journal on Uncertainty Quantification*, 1(1):452–493, 2013.

[4] KA Cliffe, MB Giles, Robert Scheichl, and Aretha L Teckentrup. Multilevel monte carlo methods and applications to elliptic pdes with random coefficients. *Computing and Visualization in Science*, 14(1):3–15, 2011.

[5] Timothy A. Davis. *Direct methods for sparse linear systems*, volume 2 of *Fundamentals of Algorithms*. Society for Industrial and Applied Mathematics (SIAM), Philadelphia, PA, 2006.

[6] J. Douglas, Jr., P. J. Paes-Leme, J. E. Roberts, and Jun Ping Wang. A parallel iterative procedure applicable to the approximate solution of second order partial differential equations by mixed finite element methods. *Numer. Math.*, 65(1):95–108, 1993.

[7] Guillermo Marshall. Monte carlo methods for the solution of nonlinear partial differential equations. *Computer physics communications*, 56(1):51–61, 1989.

[8] Bradley McCaskill. *A multiscale domain decomposition method and its application in conservation problems*. ProQuest UMI Dissertations Publishing, 2014.

[9] Nicholas Metropolis and Stanislaw Ulam. The monte carlo method. *Journal of the American statistical association*, 44(247):335–341, 1949.

[10] Yousef Saad. *Iterative methods for sparse linear systems*. Society for Industrial and Applied Mathematics, Philadelphia, PA, second edition, 2003.

[11] Dongbin Xiu and George Em Karniadakis. The wiener–askey polynomial chaos for stochastic differential equations. *SIAM journal on scientific computing*, 24(2):619–644, 2002.

[12] Zhiwen Zhang, Maolin Ci, and Thomas Y Hou. A multiscale data-driven stochastic method for elliptic pdes with random coefficients. *Multiscale Modeling & Simulation*, 13(1):173–204, 2015.